Journal of Biomechanics 141 (2022) 111218

Contents lists available at ScienceDirect

Journal of Biomechanics

journal homepage: www.elsevier.com/locate/jbiomech

Structure-function relationships in dog dentin

Jason W. Soukup [a,*], Scott J. Hetzel [b], Donald S. Stone [c], Melih Eriten [d], Heidi-Lynn Ploeg [d,e], Corinne R. Henak [d,f]

[a] Department of Surgical Sciences, University of Wisconsin-Madison, School of Veterinary Medicine, Madison, WI, USA
[b] Department of Biostatistics and Medical Informatics, University of Wisconsin-Madison, School of Medicine and Public Health, Madison, WI, USA
[c] Department of Materials Science and Engineering, University of Wisconsin-Madison, College of Engineering, Madison, WI, USA
[d] Department of Mechanical Engineering, University of Wisconsin-Madison, College of Engineering, Madison, WI, USA
[e] Department of Mechanics and Materials Engineering, Queen's University, Kingston, ON, Canada
[f] Department of Orthopedics and Rehabilitation, University of Wisconsin-Madison, School of Medicine and Public Health, Madison, WI, USA

ARTICLE INFO

Keywords:
Mechanical properties
Microstructure
Dentin
Nanoindentation
Dentinal tubules

ABSTRACT

Investigations into teeth mechanical properties provide insight into physiological functions and pathological changes. This study sought to 1) quantify the spatial distribution of elastic modulus, hardness and the microstructural features of dog dentin and to 2) investigate quantitative relationships between the mechanical properties and the complex microstructure of dog dentin. Maxillary canine teeth of 10 mature dogs were sectioned in the transverse and vertical planes, then tested using nanoindentation and scanning electron microscopy (SEM). Microstructural features (dentin area fraction and dentinal tubule density) and mechanical properties (elastic modulus and hardness) were quantified. Results demonstrated significant anisotropy and spatial variation in elastic modulus, hardness, dentin area fraction and tubule density. These spatial variations adhered to a consistent distribution pattern; hardness, elastic modulus and dentin area fraction generally decreased from superficial to deep dentin and from crown tip to base; tubule density generally increased from superficial to deep dentin. Poor to moderate correlations between microstructural features and mechanical properties ($R^2 = 0.032–0.466$) were determined. The results of this study suggest that the other constituents may contribute to the mechanical behavior of mammalian dentin. Our results also present several remaining opportunities for further investigation into the roles of organic components (e.g., collagen) and mineral content on dentin mechanical behavior.

1. Introduction

Mammalian teeth are hierarchical and heterogeneous and considered a function-oriented, bilayer composite material of enamel and dentin (Fig. 1). Enamel is 96% mineral (hydroxyapatite; HA) (Nanci, 2013b) and serves as a stiff layer to protect the tooth from the forces of mastication (R. Wang & Weiner, 1997). The underlying dentin is a porous tissue composed of dentinal tubules within a matrix, which is 70% mineral in the form of carbonated HA crystals (Nanci, 2013a). Dentinal tubules radiate from the pulp to the dentinoenamel junction (DEJ) in an s-shaped pathway. Dentin serves to absorb impacts and distribute high stresses (Chai et al., 2009). Dentinal tubules measure approximately 3 μm in diameter near the interface with the pulp and decrease to approximately 2.4 μm at the DEJ (Lopes et al., 2009). Tubule diameter in dogs is comparable to those in humans (Robb et al., 2007). Studies evaluating dentinal tubules in humans and other mammals have shown significant spatial and morphological variation within and between individuals and species (Lopes et al., 2009; Mlakar et al., 2014; Robb et al., 2007).

Investigations into teeth structure–function relationships, where function is defined by its mechanical function (i.e., mechanical properties) provide insight into the effect structure (at various length scales) has on mechanical behavior. Micro- and nanoindentation are common methods for acquiring teeth mechanical properties given the small size and the need for precision measurements (Kundanati et al., 2019; Shen et al., 2020; Yi et al., 2020; Zhang et al., 2014). The mechanical properties of enamel and, to a lesser degree, dentin have been investigated with micro- and nanoindentation and reveal that elastic modulus (E) and

* Corresponding author at: Department of Surgical Sciences, University of Wisconsin-Madison, School of Veterinary Medicine, 2015 Linden Drive, Madison, WI 53706, USA.
E-mail address: jason.soukup@wisc.edu (J.W. Soukup).

https://doi.org/10.1016/j.jbiomech.2022.111218
Accepted 4 July 2022
Available online 8 July 2022

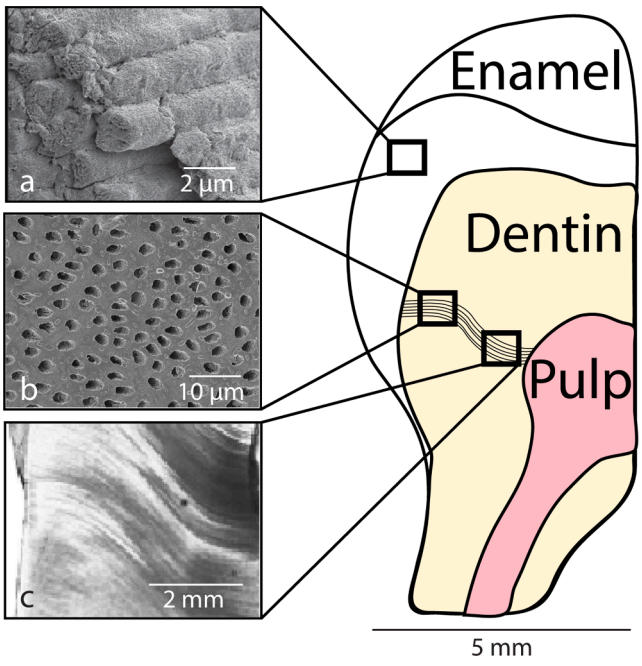

Fig. 1. Illustration of dental anatomy depicting a cross section of ½ of a human molar. Call outs of (a) SEM microstructure of human enamel (reprinted with permission via creative commons license from Pandya M, et al. Enamel biomimetics-fiction or future of dentistry. *Int J Oral Sci* 2019; 11:8.); (b) SEM microstructure of dog dentin; and (c) ground section of human dentin showing the s-shaped pathway of the dentinal tubules from the pulp to the DEJ (reprinted with permission from Snoddy AME, et al. An image analysis protocol for the quantification of interglobular dentin in anthropological tooth sections. *Am J Phys Anthropol* 2021; 174: 144–148).

hardness (*H*) *1)* decrease from the outer to the inner regions and *2)* are influenced by location and direction of testing; the direction of macro- and micro-scale features; the nature of the storage and testing hydration parameters; and the average density of the mineral phase (An et al., 2012; Ang et al., 2009, 2010; Angker et al., 2003, 2004; Barbour et al., 2003; Bertassoni & Swain, 2012; Braly et al., 2007; Chan et al., 2011; Cuy et al., 2002; Fränzel & Gerlach, 2009; Ge et al., 2005; Habelitz et al., 2001, 2002; Han et al., 2012; He et al., 2006; He & Swain, 2009; Jeng et al., 2011; Jíra & Němeček, 2014; Mahoney et al., 2000; Mahoney et al., 2004; Park et al., 2008; Ziskind et al., 2011) (Tables 1 & 2).

While previous investigations have advanced our understanding of dentin microstructure and mechanical behavior, there is not yet a complete mapping of the three-dimensional (3D) spatial distribution of mammalian dentin microstructure and the mechanical properties. This mapping would provide insight into relationships between mechanical properties and microstructure. Therefore, the aims of this study were to: *1*) quantify the 3D spatial distribution of *E, H* and microstructural features of dog dentin using nanoindentation and scanning electron microscopy; *2*) characterize the relationship between *E, H* and the microstructural features of dog dentin using nanoindentation and scanning electron microscopy.

2. Materials and methods

2.1. Sample preparation

Ten maxillary canine teeth were extracted from individual dogs euthanized for reasons unrelated to the study (Supplemental table 1), wrapped in Hanks' balanced salt solution saturated gauze, vacuum sealed and stored at −20°C. Teeth were thawed at ambient temperature for 24 h prior to submersion in a resin (Orthodontic Resin, Hygenic, Akron, OH) to create a tooth block, which were allowed to cure for 24 h.

Table 1
Published mechanical properties of human enamel.

Reference	Site	Hardness (GPa)	Elastic Modulus (GPa)
E Mahoney (2000)	1st molar	4.88 +/- 0.41	80.94 +/- 6.65
S Habelitz (2001)	3rd molar	Parallel to rod 3.9 +/- 0.3; Perpendicular to rod 3.3 +/- 0.3	Parallel to rod 87.5 +/- 2.2; Perpendicular to rod 72.7 +/- 4.5
SF Ang (2009, 2010)	3rd molar	5.7 +/- 0.3	86.4 +/- 11.7
Y-R Jeng (2011)	Premolar	4.48 +/- 0.23	92.72 +/- 3.09
JL Cuy (2002)	2nd, 3rd molar	Surface > 6; Near DEJ < 3	Surface > 115; Near DEJ < 70
ME Barbour (2003)	3rd molar	4.81 +/- 0.15	99.6 +/- 1.8
EK Mahoney (2004)	1st molar	3.66 +/- 0.75	75.57 +/- 9.98
J Ge (2005)	3rd molar	Rod 4.3 +/- 0.8; Sheath 1.1 +/- 0.3	Rod 83.4 +/- 7.1; Sheath 38.5 +/- 4.1
LH He (2006, 2009)	Premolar	Surface 5 +/- 0.45; Inner layer 3.05 +/- 0.41	Surface 60–100; Inner layer 56.8 +/- 5.39
B-B An (2012)	Molar	–	Surface 80; Inner layer 60
A Braly (2007)	3rd molar	6–7	120–130

Table 2
Published mechanical properties of human dentin.

Reference	Site	Hardness (GPa)	Elastic Modulus (GPa)
E Mahoney (2000)	1st molar	0.95 +/- 0.11	20.55 +/- 2.00
L Angker (2003)	1st molar	Pulpal interface 0.52 +/- 0.24; central region 0.85 +/- 0.19; DEJ 0.91 +/- 0.15	Pulpal interface 11.59 +/- 3.95; central region 17.06 +/- 3.09; DEJ 16.33 +/- 3.83
W Franzel (2009)	Molar	0.78 +/- 0.1	22.4 +/- 2.6
D Ziskind (2011)	3rd molar, premolar	Peritubular dentin 1.34 +/- 0.5; Intertubular dentin 0.60 +/- 0.2	Peritubular dentin 29.3 +/- 6.7; Intertubular dentin 17.4 +/- 3.5
YL Chan (2011)	Molar	1 +/- 0.1	19 +/- 2
LE Bertassoni (2012)	3rd molar	Dry environment 1.43 +/- 0.12; Hydrated environment 0.88 +/- 0.11	–
C-F Han (2012)	Molar	10° to dentinal tubule 0.588; 80° to dentinal tubule 0.521	10° to dentinal tubule 16.15; 80° to dentinal tubule 13.28

The crowns of 5 teeth were sectioned with a Leica SP1600 high-precision, diamond histological saw into five transverse sections of equal thickness. The crowns of the remaining 5 teeth were sectioned into three vertical crown sections (Fig. 2). Sections were ground with 400, 600, 800 and 1200 grit silicon-carbide sandpaper on a water-cooled, low-speed benchtop grinder/polisher (Ecomet III, Beuhler, Lake Bluff, IL). Sequential polishing with 6, 1 and 0.25 µm diamond suspensions was then performed. Between polishings, all samples were rinsed for 1 min with distilled water. Samples were stored in Hanks' balanced salt solution at ambient temperature until ready for nanoindentation testing (<48 hrs.).

2.2. Nanoindentation testing

Cross sections were adhered to magnetic pucks with cyanoacrylate (Superglue, Loctite, Westlake, OH). Spatially variant mechanical properties of dentin were evaluated using nanoindentation with a TI 950 Triboindenter (Bruker, Minneapolis, MN). On *transverse cross sections*, 10

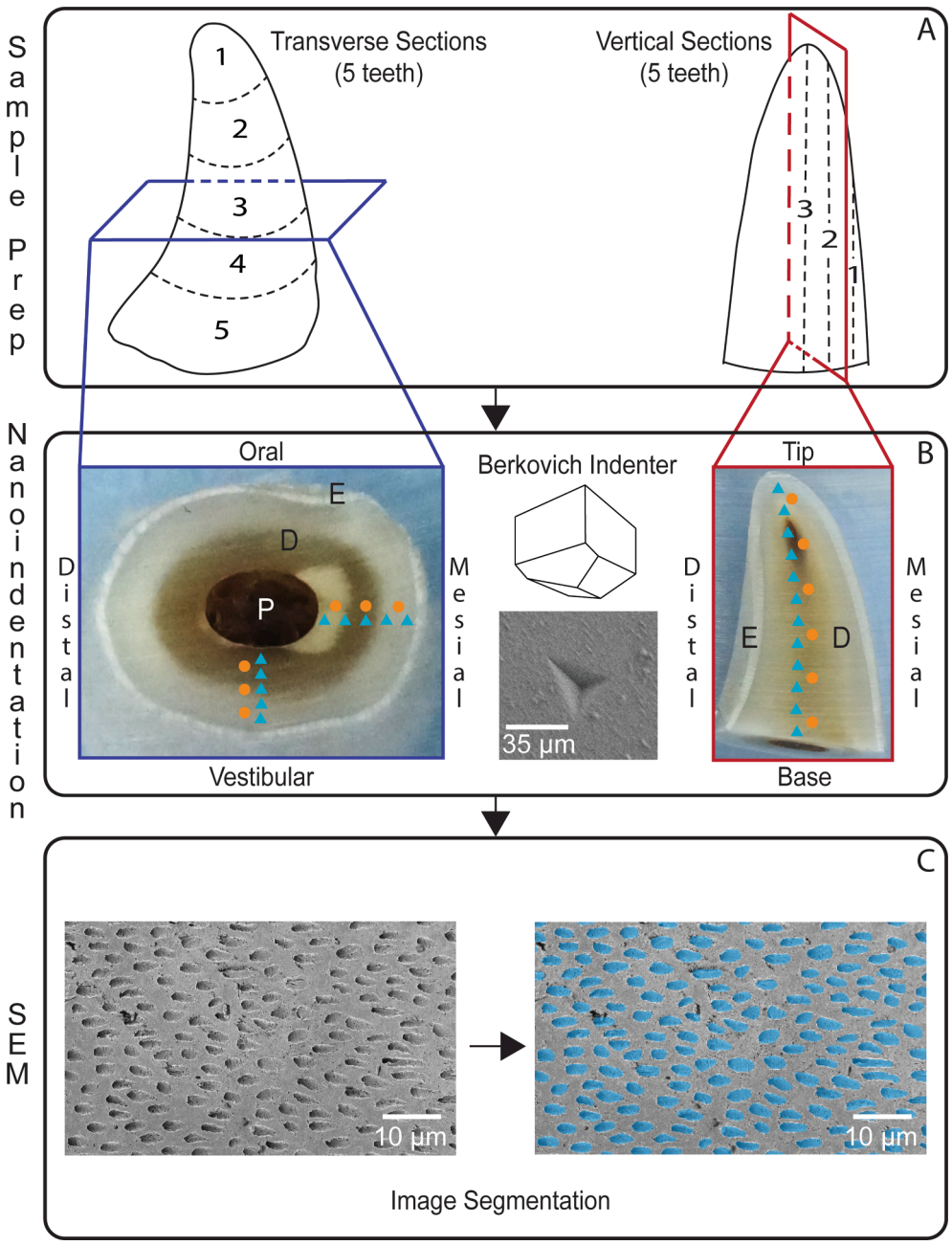

Fig. 2. Overview of experimental design. Blue box (left) represents transverse sections and red box (right) represents vertical sections. Blue triangles represent locations of nanoindentation data and orange circles represent locations of SEM image acquisition. Note the light microscopic image of a nanoindentation location from the present study in the nanoindentation (middle) box representing the typical contact area of the indentations. P = pulp; D = dentin; E = enamel. In panel C, completion of image segmentation results in dentinal tubule phase highlighted in blue.

indentations were made [five from the dentinoenamel junction (DEJ) to the pulpal interface in the vestibulo-oral (VO) direction and five from the pulpal interface to the DEJ in the disto-mesial (DM) direction]. In the *vertical cross sections*, 6–12 indentations were made from the crown base to the crown tip as determined by the length of the resulting section (Fig. 2). All indentations were made with a TI-0083 high-load Berkovich indenter (Bruker, Minneapolis, MN) on a high-load transducer using a controlled displacement to 5000 nm with a 5 sec load and 5 sec unload time. Load and displacement were continuously recorded at 200 Hz. Load-displacement data were used to derive E and H using the Oliver-Pharr method (Oliver & Pharr, 2004, 1992). Light microscopy was performed to confirm placement of indents in the target location. A 'SYS' plot analysis was performed to screen for structural compliance (Jakes et al., 2008).

2.3. Scanning electron microscopy

All samples were prepared for SEM with superficial demineralization with a 10 s rinse in 17% EDTA followed by a 1-minute rinse in distilled water. Deproteination was achieved with a 1-minute bath in 50% NaHOCl followed by a 1-minute rinse in distilled water. The samples were dehydrated through a series of 20-minute immersions in ethanol solutions of increasing concentration (25, 50, 75, 95 and 100%). Samples were dried under ambient conditions for 10 min prior to storage in a desiccant chamber for 24 h. Samples were then adhered to SEM pins and sputter-coated with 10 nm thick coating of gold (Leica EM ACE600, Leica Microsystems, Buffalo Grove, IL).

Samples were imaged with a high-vacuum SEM (LEO 1530, Zeiss Microscopy, White Plains, NY) at an accelerating voltage of 10 kV and a working distance of 30 mm. Six images were acquired for each transverse cross section at locations corresponding with the DEJ, the mid-dentin region and the inner dentin region near the pulpal interface in

both the VO and the DM directions. Between three and 13 images were acquired for each vertical cross section corresponding approximately with the nanoindentation locations from the crown base to the crown tip.

2.4. Image processing and analysis

Individual SEM image files were imported into an image processing software (Dragonfly v2021.1, Object Research Systems, Montreal, Quebec). Images were segmented into two classes (dentinal tubules and intertubular dentin). Segmentation was performed either manually or with a segmentation trainer based on image quality, image heterogeneity and tubule density (TD) (Details provided in online supplemental materials). The dentinal tubule class for each image was then converted into a new dataset that identified each individual dentinal tubule as a separate object. This step allowed calculation of image TD as tubules/mm^2. Image dentin area fraction (ratio of dentin area to overall surface area; DAF) is reported as a percentage. All segmentation was completed by one operator (JWS).

2.5. Statistical analysis

For the purposes of analyzing correlation between mechanical properties and microstructural features, a normalization procedure to match nanoindentation position with SEM image acquisition position was performed (Details provided in online supplemental materials). The statistical assessment of correlation after the normalization process involved fitting linear mixed effects (LME) regression models with the two variables of interest as the outcome (*E* or *H*) and fixed effect predictor (DAF or TD) with a random nested effect of Section within Tooth. TD was determined to have a skewed right distribution and therefore a base e log-transformation of this variable was used to normalize the distribution. The LME model was run individually for all four 2-way combinations of the outcomes and predictors and separately for transverse and vertical directions. Correlation is then estimated as the coefficient of determination (R^2) from the LME model. This distribution pattern for *E* and *H* in the transverse sections was mirrored between the VO and DM directions. Given the mirrored pattern, analogous positions in the VO and DM directions were combined for statistical analysis. Estimation of mean (95% CI) for each Section required fitting individual mixed effects ANOVA models with *E*, *H*, DAF, or TD as the outcome, Section as a fixed factor variable, and Tooth as a random effect. A similar analysis method was used for estimating mean (95% CI) for each Position with Position as the fixed factor variable and the rest of the model structure staying the same. This process was done separately in both the transverse and vertical directions. If the ANOVA p-value was significant then two-way post-hoc analyses with Tukey's family-wise correction was used through the implementation of the emmeans function in R. All analyses were conducted in R for statistical computing v4.0.

3. Results

3.1. Samples

A total of 10 tooth samples are reported from 10 dogs (Supplemental Table 1). After light microscopic and 'SYS' plot analysis, 40 and 15 datapoints from transverse and vertical sections, respectively, were excluded due to evidence of poor indentation location or structural compliance. The remaining 210 and 128 datapoints from transverse and vertical sections, respectively, were available for analysis. Sixteen and nine SEM images were excluded from the transverse and vertical sections, respectively, due to unacceptable resolution, leaving 134 transverse and 79 vertical section images available for microstructure analysis. The correlation analysis normalization process resulted in 110 and 50 datapoints available for the transverse and vertical cross section analyses, respectively.

3.2. Mechanical properties

3.2.1. Elastic modulus

Elastic modulus ranged widely (Supplemental Table 2), was anisotropic and heterogeneous. Structural anisotropy was appreciated with higher mean modulus in transverse than in vertical sections ($p < 0.001$). In transverse sections, the mean modulus decreased from the DEJ to the pulpal interface ($p < 0.001$) (Fig. 3A). *E* in the position immediately adjacent to the DEJ was lower than the position adjacent to it. Additionally, *E* significantly increased from the crown base to the crown tip ($p < 0.001$) (Fig. 3B). *E* increased slightly ($p = 0.259$) from the outer vertical section (nearest DEJ) to the inner vertical section (nearest pulpal interface) (Fig. 3C). *E* increased in vertical sections ($p < 0.001$) from the crown base to crown tip with the position nearest the DEJ revealing a slight decrease (Fig. 3D).

3.2.2. Hardness

Significant variation was found in *H*. The values in the transverse sections were not significantly different than those in the vertical sections, suggesting any possible anisotropy in *H* was too small to be detected using nanoindentation. In general, the distribution pattern followed that of *E* for both transverse and vertical sections. A statistically significant trend ($p < 0.001$) was observed with *H* decreasing from the DEJ to the pulpal interface in the transverse sections (Fig. 4A). *H* also increased ($p < 0.001$) from the crown base to the crown tip in the vertical sections (Fig. 4C). This pattern ($p = 0.004$) can also be appreciated by the difference in the mean transverse sectional values of sections 1 and 5 (Fig. 4B). *H* in the outer vertical section was lower relative to the middle region and similar in value to the inner vertical section (Fig. 4D). The outer and central vertical sections and the central and inner vertical sections were significantly different ($p = 0.015$ and $p = 0.009$, respectively).

3.3. Microstructural features

3.3.1. Dentin area fraction

Like *E* and *H*, DAF decreased from the DEJ to the pulpal interface in the VO and DM directions (Fig. 5A). However, unlike *E* and *H*, DAF did not differ from crown base to tip ($p = 0.680$) (Fig. 5B). The distribution pattern for vertical sections was similar to those in the transverse sections. DAF in the outer vertical section was not significantly different from the middle region ($p = 0.586$) but the middle region was higher than the inner vertical section ($p < 0.001$) (Fig. 5C). The outer and middle vertical sections and the middle and inner vertical sections were significantly different from one another, respectively ($p=<0.001$). DAF generally increased from the crown base to the crown tip (Fig. 5D). A corresponding drop in DAF was noted near the DEJ at the crown tip.

3.3.2. Tubule density

TD increased ($p < 0.001$) from the DEJ to the pulpal interface in the VO and the DM directions (Fig. 6A). TD significantly increased from crown base to crown tip ($p = 0.026$) (Fig. 6B). These trends continued in the vertical sections. TD in the outer vertical section was lower compared to the central region and the central region was lower than the inner vertical section (Fig. 6C). The differences between vertical sections were not significant. TD for the vertical sections also suggested a trend of decreasing TD from the crown base to the crown tip (Fig. 6D).

3.4. Correlations between mechanical properties and microstructural features

There were poor to moderate correlations between mechanical properties and microstructural features (Figs. 7 and 8). Most correlations [TD/*E* (transverse); TD/*H* (transverse); DAF/*E* (transverse); DAF/*H* (transverse); DAF/*H* (vertical)] were statistically significant but with low R-squared values ($p < 0.05$; R-squared > 0.4). Higher correlation

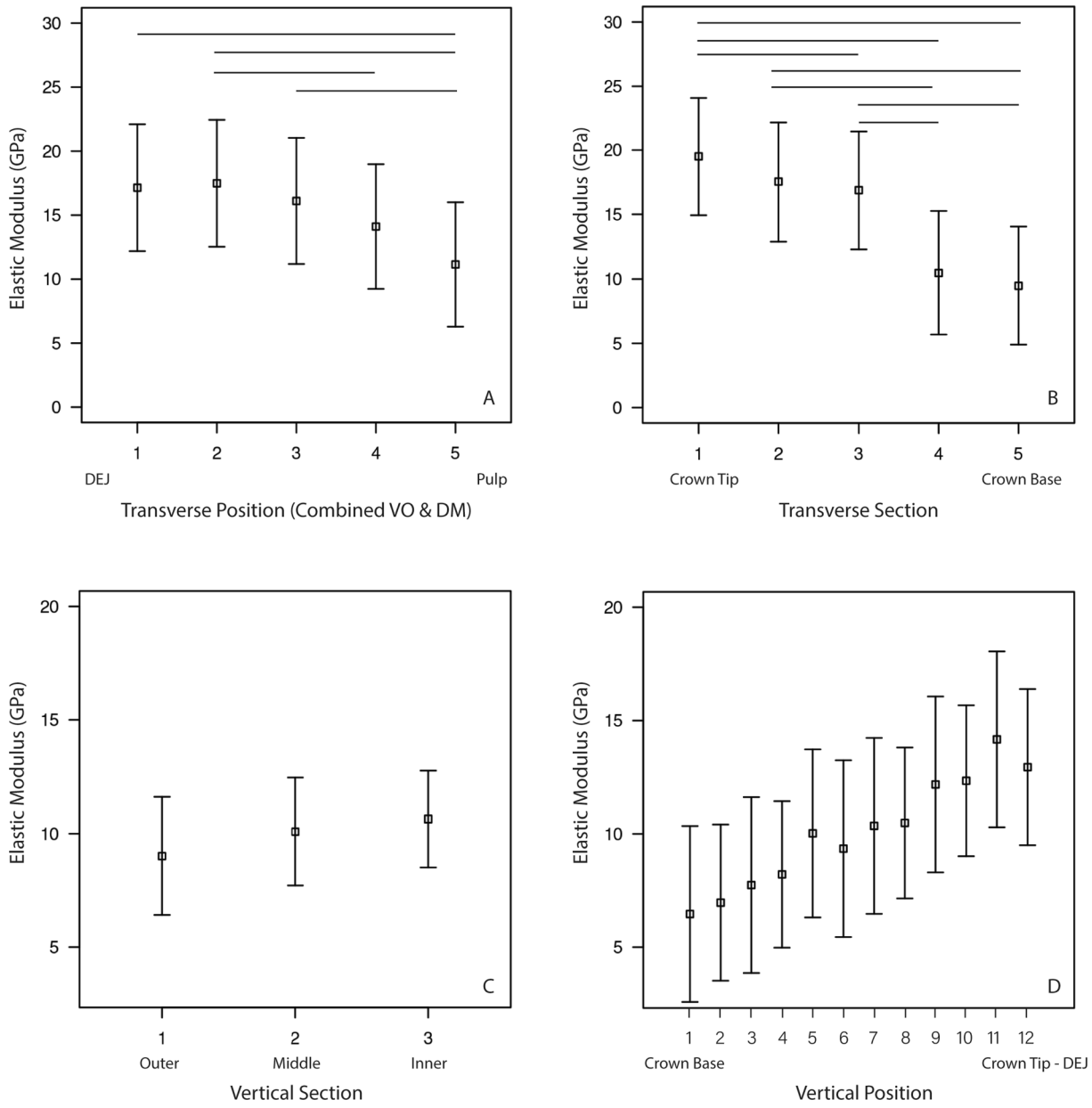

Fig. 3. Mean and 95% confidence intervals for *E* as a function of combined transverse positions (A), transverse section (B), vertical section (C) and vertical position (D). For plots A and B, significance between positions and sections are noted with solid bars. Note the trend of increasing *E* from the crown base to the crown tip in plots B and D. In plots A and D, note the slight decrease in *E* near the DEJ.

was found between DAF and *H/E* [$R^2 = 0.437$ and 0.466 for DAF/*E* and DAF/*H*, respectively] in transverse sections as compared to DAF and *H/E* [$R^2 = 0.129$ and 0.213 for DAF/*E* and DAF/*H*, respectively] in vertical sections (Fig. 8). While correlation between mechanical properties and TD was higher in transverse sections compared to vertical sections and higher for *H* than for *E*, these correlations were poor [$R^2 = 0.032$ (vertical sections – *E*/TD); =0.346 (transverse sections – *H*/TD)] (Fig. 8).

4. Discussion

This study achieved our aims, demonstrating anisotropy and heterogeneity of, and characterizing the relationship between, *E; H*; and microstructural features of dog dentin.

4.1. Heterogeneity in mechanical properties

H and *E* decreased from the DEJ to the pulp and from the crown tip to the base with a decrease adjacent to the DEJ. These patterns are consistent with previous studies in human dentin (Jíra & Němeček, 2014; R. Z. Wang & Weiner, 1997). The slight decrease adjacent to the DEJ may be explained by the presence of dentin phosphoproteins that are largely unphosphorylated (Reed et al., 2015; R. Wang & Weiner, 1997). The wide range of values found in the literature and reported here may be explained by differences in sectioning specimens, specimen surface imperfections and individual subject variance (e.g., differences in mineralization during odontogenesis) (Angker et al., 2003). Due to the sigmoid path of the dentinal tubule, indentations are invariably performed in samples with varying tubule orientation, which has been shown to affect mechanical property measurements (Watanabe et al., 1996).

In the present study, TD ranged widely depending on location and orientation of the cross section evaluated. The upper end of the range is substantially higher than those values previously reported in human dentin and dog dentin (Carrigan et al., 1984; Dourda et al., 1994; Fosse

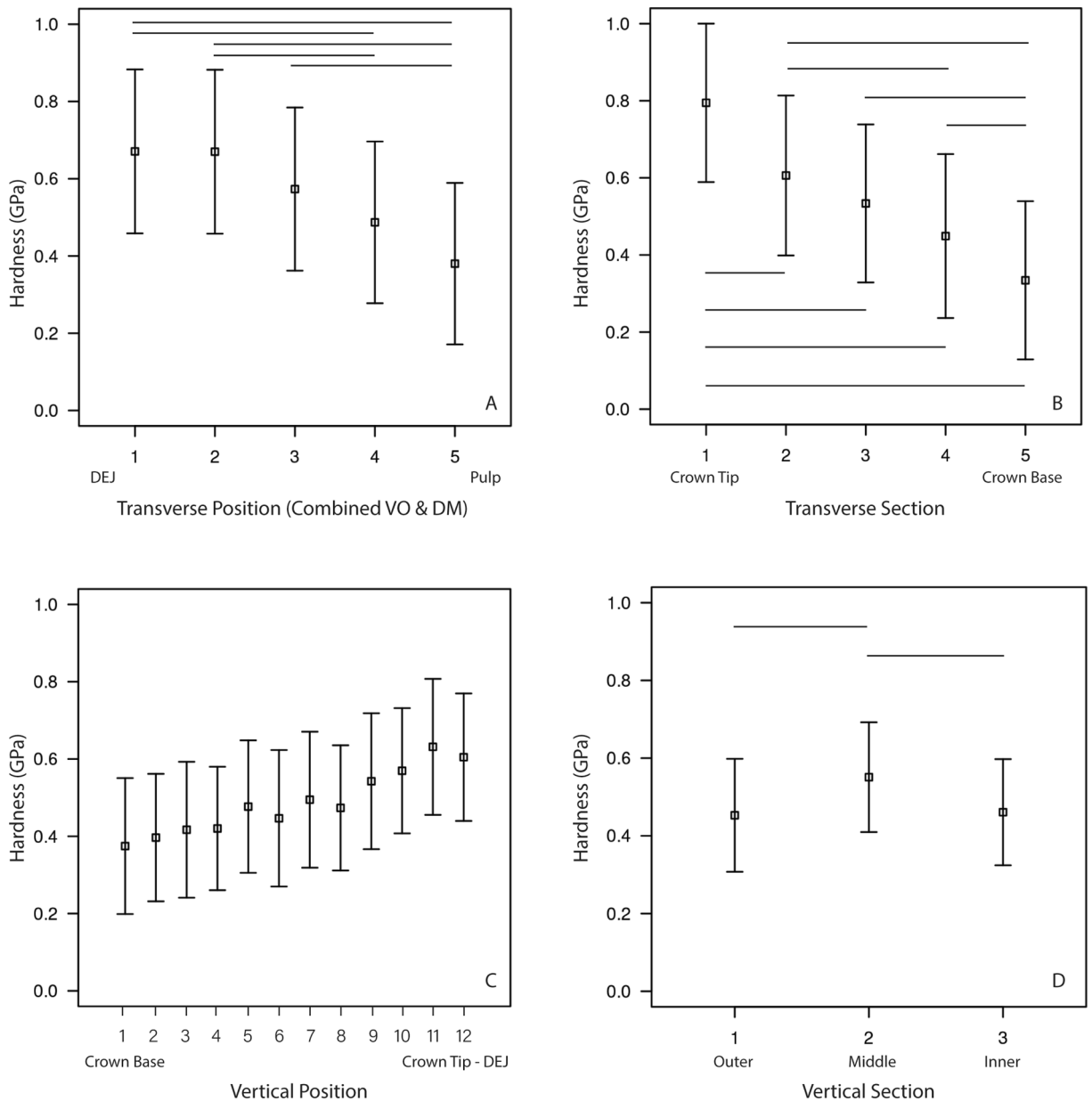

Fig. 4. Mean and 95% confidence intervals for H as a function of combined transverse positions (A), transverse section (B), vertical position (C) and vertical section (D). Significance between positions and sections is noted with solid bars. Note the trend of increasing H from the crown base to the crown tip in plots B and C.

et al., 1992; Garberoglio & Brannstrom, 1976; Ketterl, 1961; Koutsi et al., 1994; Mjör & Nordahl, 1996; Olsson et al., 1993; Pashley et al., 1985; Robb et al., 2007; Schilke et al., 2000; Tronstad, 1973; Whittaker & Kneale, 1979). TD increased as a function of distance from the DEJ in both transverse and vertical sections and from the crown base to tip. DAF increased as a function of distance from the pulp in both transverse and vertical sections. DAF decreased in a coronoapical direction. Our findings are consistent with previous reports in human and dog dentin (Carrigan et al., 1984; Marshall et al., 1997; Robb et al., 2007; Whittaker & Kneale, 1979). Due to differences in methodology, species, teeth and testing regions, it is difficult to directly compare our results to previous studies. Dog dentin TD at the crown base has been reported to be ~ 30,000/mm^2-~47,000/mm^2 for superficial and deep dentin, respectively (Robb et al., 2007). This is higher than the values in our study. However, previous studies measured only at the crown base and have only evaluated TD in a few locations. Our study characterized dentin microstructural features of the entire tooth volume in multiple planes and sections.

4.2. Anisotropy in mechanical behavior

Evidence of anisotropy in the mechanical properties was found. Dentin anisotropy may be anticipated when modeled as a two phase biocomposite in which peritubular dentin associated with the dentinal tubules is a hollow fiber, surrounded by the intertubular dentin matrix (Angker et al., 2003). When tested parallel to the direction of the fiber E can be defined by the Voigt composite model (Voigt, 1889).

$$E_c = E_1 V_1 + E_2 V_2 \tag{1}$$

and when tested perpendicular to the fiber, E can be defined by the Reuss composite model (Reuss, 1929).

$$\frac{1}{E_c} = \frac{V_1}{E_1} + \frac{V_2}{E_2} \tag{2}$$

where E_c is the composite elastic modulus, E_1 and V_1 are the elastic modulus and volume fraction of the first constituent, respectively and E_2

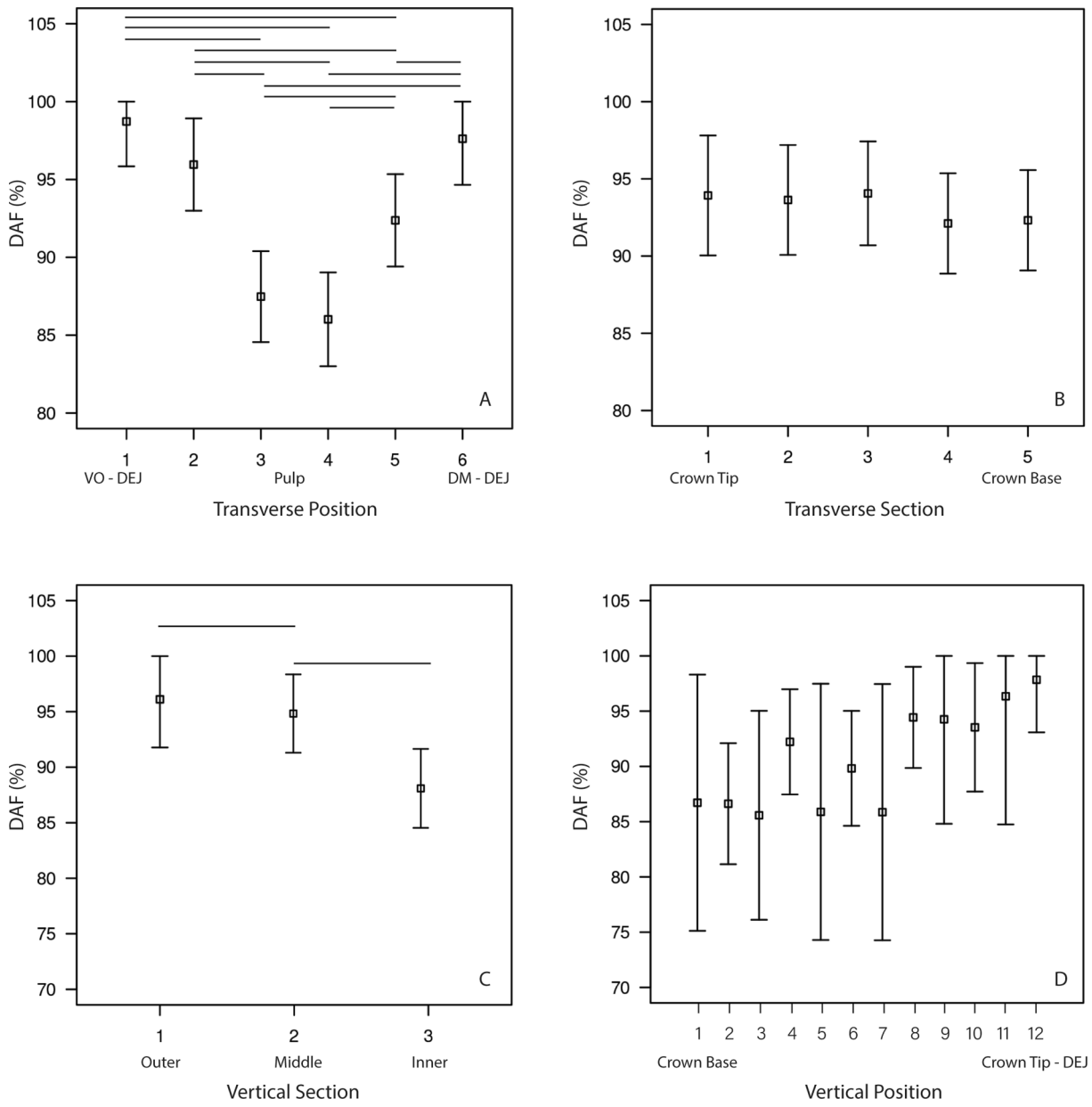

Fig. 5. DAF as a function of transverse position (A); transverse section (B); vertical section (C); and vertical position (D). Significant differences between variables are marked with a solid bar.

and V_2 are the elastic modulus and volume fraction of the second constituent, respectively (Ashby & Jones, 2013; Mencik, 1992). These models predict that E will be different (potentially orders of magnitude different) depending on the testing direction. These simple models, however, are not perfectly suited to the complex hierarchical structure of dentin. Models attempting to account for the complexity of dentin have been employed with varying degrees of success (Bar-On & Daniel Wagner, 2012; Biswas et al., 2013; Kinney et al., 1999; Qin & Swain, 2004; Wang & Qin, 2007). Most models still assume dentinal tubules to be isotropic, cylindrical inclusions with a non-tortuous path. In reality, indentation test direction will not be perfectly parallel or perpendicular to the dentinal tubules as assumed in the models. Also, because individual nanoindentation positions in vertical sections did not necessarily correlate with individual positions in transverse sections, a paired analysis could not be performed. Thus, while the transverse and vertical values reported here are evidence of anisotropy, they may not necessarily reflect the true nature of that anisotropy.

4.3. Correlations between mechanical properties and microstructural features

Within the limitations of the data reported here (i.e., limited to structural features of DAF and tubule density), our results, the first to attempt structure–function correlations in dog dentin, suggest the correlation between mechanical properties and microstructural features in dog dentin are poor to moderate. The strongest correlations were present between H/E and DAF in transverse sections. These correlations suggest that microstructure contributes to but is not the sole driver of dentin mechanical properties. Other investigators have suggested that the mechanical properties of dentin are largely driven by the microstructural features (Craig et al., 1959; Fusayama et al., 1966; Garberoglio & Brännström, 1976; Pashley et al., 1985). Human molar dentin microhardness and TD are strongly correlated (Pashley et al., 1985). While the distribution of DAF and TD are related to the mineralization gradient throughout the tooth, one does not necessarily depend on the other. For example, the DAF near the DEJ is high, yet the mechanical

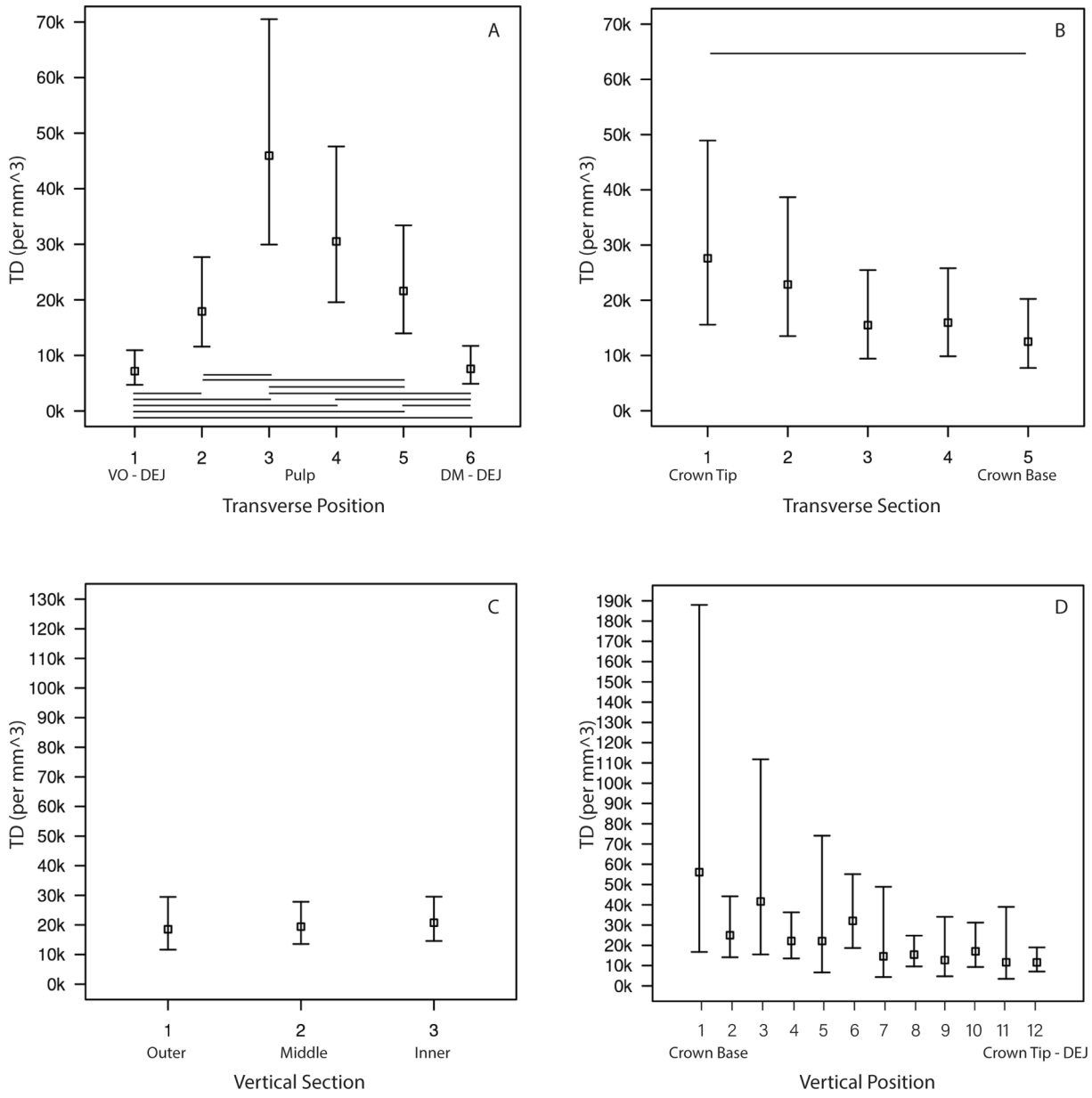

Fig. 6. Plots depicting TD as a function of transverse position (A); transverse section (B); vertical section (C); and vertical position (D). Significant differences between variables are marked with a solid bar. Note, significant differences are from p-values calculated on base e log-transformed data.

properties decrease in this region, likely due to a slightly lower mineral content (MacDougall et al., 1992). Mineral content is a significant contributor to mechanical behavior. Demineralization of enamel and dentin have been correlated with degradation of mechanical properties (Angker et al., 2004; Zafar & Ahmed, 2015). For example, *H/E* and mineral content correlate in demineralized carious dentin (Angker et al., 2004). When dentin is exposed to phosphoric acid, a demineralizing agent used as a pretreatment in restorative dentistry, *H* is significantly reduced (Zafar & Ahmed, 2015). Dentin, however, in not a purely mineralized tissue. The organic constituent (primarily type 1 collagen) is approximately 33% (Nanci, 2013a). Collagen fibers also contribute to the mechanical properties of dentin (Ryou et al., 2012). An increase in *E* in irradiated teeth corresponds with a decrease in dentin protein/mineral ratio (Reed et al., 2015). The results of this and other studies suggest that the other constituents may hold influence over the mechanical behavior of mammalian dentin.

4.4. Limitations

Some study limitations are relevant to consider. We used an indenter with a large contact area to minimize the chance of an indent contacting only one constituent (intertubular dentin or dentinal tubule). However, while this is unlikely, it is possible some indents were not distributed across both constituents and may have contributed to the poor correlation between mechanical properties and microstructural features. Similarly, the large contact area of the indenter used in this study served to spread contact across *peri*-tubular dentin (the dentin immediately surrounding the dentinal tubule) and the rest of the intertubular dentin. As such, differences between these two constituents were likely neutralized (see supplemental material for additional discussion). While our samples were hydrated until the moment of nanoindentation testing, no efforts were made to maintain hydration during testing. It is possible that the samples began to lose hydration during testing. Others have shown that hydrated dentin has lower *H* and *E* values compared to dehydrated dentin (Bajaj et al., 2006; Balooch et al., 1998; Jameson

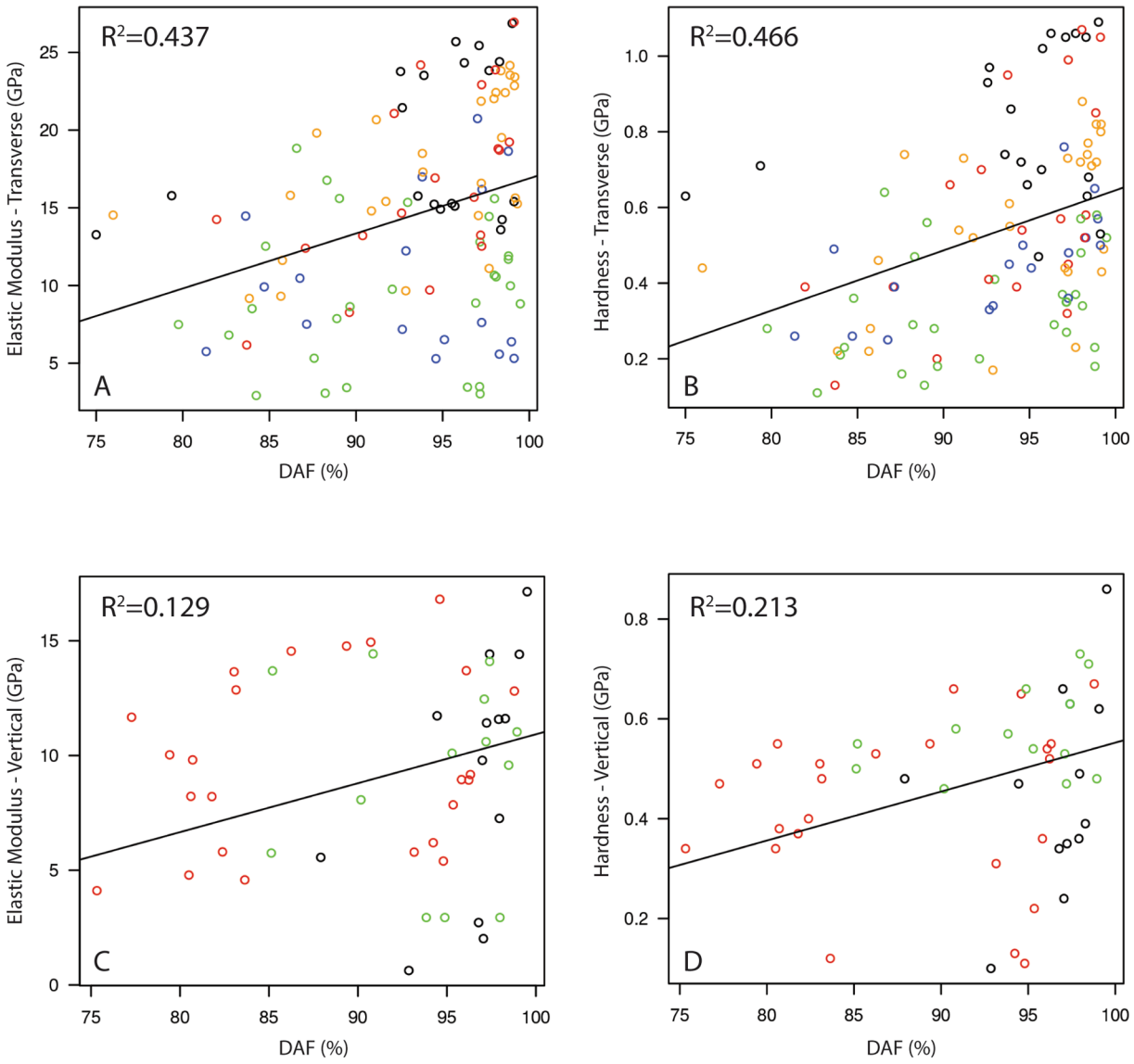

Fig. 7. Linear regression plots depicting the correlation between transverse section *E* and DAF (A); between transverse section *H* and DAF (B), between vertical section *E* and DAF (C); and between vertical section *H* and DAF (D). For plots A and B, transverse cross sections are color-coded; black circles = section 1 (crown tip), red circles = section 2, yellow circles = section 3, blue circles = section 4, green circles = section 5 (crown base). For plots C and D, vertical cross sections are color-coded; black circles = section 1 (near DEJ), green circles = section 2, red circles = section 3 (near pulp).

et al., 1993; Kahler, 2008; Kruzic et al., 2003; Ryou et al., 2012). In addition, our analysis of structure–function relationships focused on the structural features of DAF and tubule density. Other important structural features of dentin, such as arrangement of tubules, morphology of peritubular dentin and structural hierarchy were not evaluated but may play a critical role in such relationships (Ji & Gao, 2004). The SEM sample prep process may have altered the morphology of the exposed dentinal tubules, which could have introduced error to the dentinal tubule and DAF measurements. To improve SEM resolution, all samples underwent superficial demineralization with a brief EDTA rinse. Despite this, final resolution results were sub-optimal, which could have altered the image segmentation process to effect DAF and tubule density values. In addition, the use of the same samples for nanoindentation and SEM image acquisition, necessary to correlate data, introduced some challenges. We were unable to acquire an SEM image for each individual nanoindentation location. The normalization process used to match locations may have introduced error in our correlation analysis.

5. Conclusions

The information in the present study provides insight into fundamental structure–function relationships that would inform investigative modeling. Our results show that the mechanical properties of dog dentin are heterogeneous, reveal anisotropy and are consistent with human dentin. In addition, the microstructural features vary significantly, and the distribution pattern resembles that of human dentin. Dentin mechanical properties and microstructure are moderately correlated with the best correlations between *E/H* and DAF. Our results also present several remaining opportunities for further investigation into the roles of other constituents (e.g., collagen/mineral content) on dentin mechanical behavior.

Author contributions

All authors of this work have made substantial contributions to all the following: (1) the conception and design of the study, or acquisition of data, or analysis and interpretation of data, ting the article or revising

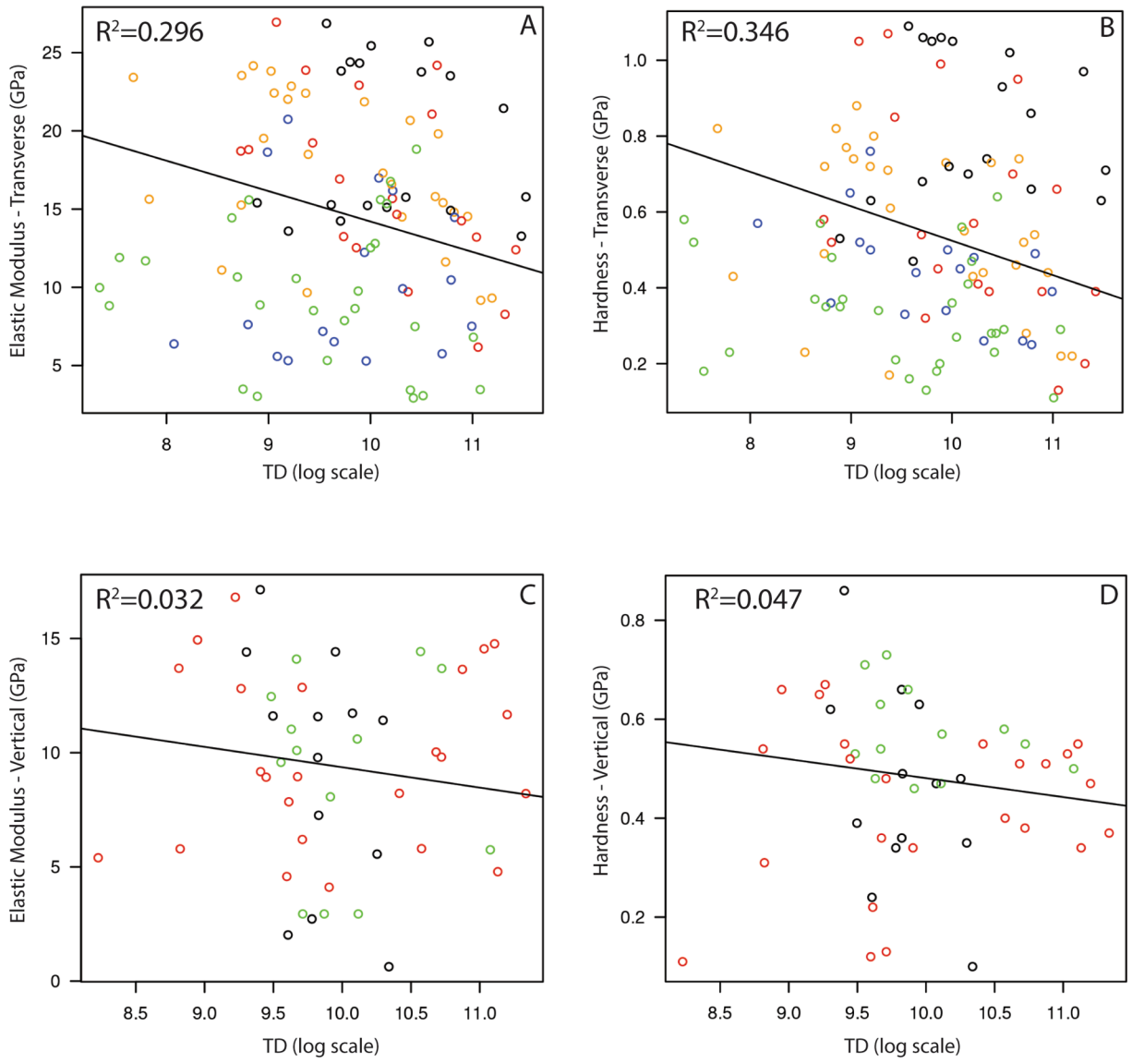

Fig. 8. Linear regression plots depicting the correlation between transverse section *E* and TD (A); between transverse section *H* and TD (B), between vertical section *E* and TD (C); and between vertical section *H* and TD (D). For plots A and B, transverse cross sections are color-coded; black circles = section 1 (crown tip), red circles = section 2, yellow circles = section 3, blue circles = section 4, green circles = section 5 (crown base). For plots C and D, vertical cross sections are color-coded; black circles = section 1 (near DEJ), green circles = section 2, red circles = section 3 (near pulp).

it critically for important intellectual content and (3) final approval of the version to be submitted.

CRediT authorship contribution statement

Jason W. Soukup: Writing – review & editing, Writing – original draft, Visualization, Validation, Supervision, Software, Resources, Project administration, Methodology, Investigation, Funding acquisition, Formal analysis, Data curation, Conceptualization. **Scott J. Hetzel:** Writing – review & editing, Writing – original draft, Methodology, Formal analysis. **Donald S. Stone:** Writing – review & editing, Supervision, Methodology, Formal analysis, Data curation. **Melih Eriten:** Writing – review & editing, Methodology, Conceptualization. **Heidi-Lynn Ploeg:** Writing – review & editing, Supervision, Software, Resources, Methodology, Conceptualization. **Corinne R. Henak:** Writing – review & editing, Visualization, Supervision, Resources, Methodology, Formal analysis, Data curation, Conceptualization.

Declaration of Competing Interest

The authors declare that they have no known competing financial interests or personal relationships that could have appeared to influence the work reported in this paper.

Acknowledgement

This project was supported by funding from the Institutional Clinical and Translational Science Award UL1 TR002373 and by the University of Wisconsin Carbone Cancer Center Support Grants P30 CA014520 and NCI P30 CA014520. The authors gratefully acknowledge use of facilities and instrumentation at the UW-Madison Wisconsin Centers for Nanoscale Technology partially supported by the NSF through the University of Wisconsin Materials Research Science and Engineering Center Grant DMR-1720415. We would like to thank and acknowledge the intellectual and technical contributions of Justin Jeffery of the UW-Madison Small Animal Imaging and Radiotherapy Facility; and Anna Kiyanova, Richard Noll and Dr. Julie Morasch of the UW-Madison Wisconsin

Centers for Nanoscale Technology.

Appendix A. Supplementary material

Supplementary data to this article can be found online at https://doi.org/10.1016/j.jbiomech.2022.111218.

References

An, B., Wang, R., Arola, D., Zhang, D., 2012. The role of property gradients on the mechanical behavior of human enamel. J. Mech. Behav. Biomed. Mater. 9, 63–72. https://doi.org/10.1016/j.jmbbm.2012.01.009.

Ang, S.F., Bortel, E.L., Swain, M.V., Klocke, A., Schneider, G.A., 2010. Size-dependent elastic/inelastic behavior of enamel over millimeter and nanometer length scales. Biomaterials 31 (7), 1955–1963.

Ang, S.F., Scholz, T., Klocke, A., Schneider, G.A., 2009. Determination of the elastic/plastic transition of human enamel by nanoindentation. Dent. Mater. 25 (11), 1403–1410. https://doi.org/10.1016/j.dental.2009.06.014.

Angker, L., Nockolds, C., Swain, M.V., Kilpatrick, N., 2004. Correlating the mechanical properties to the mineral content of carious dentine - A comparative study using an ultra-micro indentation system (UMIS) and SEM-BSE signals. Arch. Oral Biol. 49 (5), 369–378.

Angker, L., Swain, M.V., Kilpatrick, N., 2003. Micro-mechanical characterisation of the properties of primary tooth dentine. J. Dent. 31 (4), 261–267.

Ashby, M.F., Jones, D.R.H., 2013. Engineering Materials 2: An Introduction to Microstructures, Processing and Design: Second Edition. In: Engineering Materials 2: An Introduction to Microstructures, Processing and Design: Second Edition. 10.1016/C2009-0-25977-0.

Bajaj, D., Sundaram, N., Nazari, A., Arola, D., 2006. Age, dehydration and fatigue crack growth in dentin. Biomaterials 27 (11), 2507–2517. https://doi.org/10.1016/j.biomaterials.2005.11.035.

Balooch, M., Wu-Magidi, I.-C., Balazs, A., Lundkvist, A.S., Marshall, S.J., Marshall, G.W., Siekhaus, W.J., Kinney, J.H., 1998. Viscoelastic properties of demineralized human dentin measured in water with atomic force microscope (AFM)-based indentation. J. Biomed. Mater. Res. 40 (4), 539–544.

Barbour, M.E., Parker, D.M., Jandt, K.D., 2003. Enamel dissolution as a function of solution degree of saturation with respect to hydroxyapatite: a nanoindentation study. J. Colloid Interface Sci. 265 (1), 9–14. https://doi.org/10.1016/s0021-9797(03)00087-0.

Bar-On, B., Daniel Wagner, H., 2012. Enamel and dentin as multi-scale bio-composites. J. Mech. Behav. Biomed. Mater. 12, 174–183. https://doi.org/10.1016/j.jmbbm.2012.03.007.

Bertassoni, L.E., Swain, M.V., 2012. Influence of hydration on nanoindentation induced energy expenditure of dentin. J. Biomech. 45 (9), 1679–1683. https://doi.org/10.1016/j.jbiomech.2012.03.021.

Biswas, N., Dey, A., Kundu, S., Chakraborty, H., Mukhopadhyay, A.K., 2013. Mechanical Properties of Enamel Nanocomposite. ISRN Biomaterials 2013, 1–15. https://doi.org/10.5402/2013/253761.

Braly, A., Darnell, L.A., Mann, A.B., Teaford, M.F., Weihs, T.P., 2007. The effect of prism orientation on the indentation testing of human molar enamel. Arch. Oral Biol. 52 (9), 856–860. https://doi.org/10.1016/j.archoralbio.2007.03.005.

Carrigan, P.J., Morse, D.R., Furst, M.L., Sinai, I.H., 1984. A scanning electron microscopic evaluation of human dentinal tubules according to age and location. J. Endodontics 10 (8), 359–363.

Chai, H., Lee, J.J.W., Constantino, P.J., Lucas, P.W., Lawn, B.R., 2009. Remarkable resilience of teeth. PNAS 106 (18), 7289–7293. https://doi.org/10.1073/pnas.0902466106.

Chan, Y.L., Ngan, A.H.W., King, N.M., 2011. Nano-scale structure and mechanical properties of the human dentine-enamel junction. J. Mech. Behav. Biomed. Mater. 4 (5), 785–795. https://doi.org/10.1016/j.jmbbm.2010.09.003.

Craig, R.G., Gehring, P.E., Peyton, F.A., 1959. Relation of Structure to the Microhardness of Human Dentin. J. Dent. Res. 38 (3), 624–630.

Cuy, J.L.L., Mann, A.B.B., Livi, K.J.J., Teaford, M.F.F., Weihs, T.P.P., 2002. Nanoindentation mapping of the mechanical properties of human molar tooth enamel. Arch. Oral Biol. 47 (4), 281–291. https://doi.org/10.1016/S0003-9969(02)00006-7.

Dourda, A.O., Moule, A.J., Young, W.G., 1994. A morphometric analysis of the cross-sectional area of dentine occupied by dentinal tubules in human third molar teeth. Int. Endod. J. 27 (4), 184–189. https://doi.org/10.1111/j.1365-2591.1994.tb00252.x.

Fosse, G., Saele, P.K., Eide, R., 1992. Numerical density and distributional pattern of dentin tubules. Acta Odontol. Scand. 50 (4), 201–210. https://doi.org/10.3109/00016359209012764.

Fränzel, W., Gerlach, R., 2009. The irradiation action on human dental tissue by X-rays and electrons–a nanoindenter study. Z. Med. Phys. 19 (1), 5–10. https://doi.org/10.1016/j.zemedi.2008.10.009.

Fusayama, T., Okuse, K., Hosoda, H., 1966. Relationship between Hardness, Discoloration, and Microbial Invasion in Carious Dentin. J. Dent. Res. 45 (4), 1033–1046.

Garberoglio, R., Brännström, M., 1976. Scanning electron microscopic investigation of human dentinal tubules. Archs Oral Biol 21 (6), 355–362.

Ge, J., Cui, F.Z., Wang, X.M., Feng, H.L., 2005. Property variations in the prism and the organic sheath within enamel by nanoindentation. Biomaterials 26 (16), 3333–3339. https://doi.org/10.1016/j.biomaterials.2004.07.059.

Habelitz, S., Marshall, G.W., Balooch, M., Marshall, S.J., 2002. Nanoindentation and storage of teeth. J. Biomech. 35 (7), 995–998. https://doi.org/10.1016/S0021-9290(02)00039-8.

Habelitz, S., Marshall, S.J., Marshall, G.W.J., Balooch, M., 2001. Mechanical properties of human dental enamel on the nanometre scale. Arch. Oral Biol. 46 (2), 173–183. https://doi.org/10.1016/s0003-9969(00)00089-3.

Han, C.-F., Wu, B.-H., Chung, C.-J., Chuang, S.-F., Li, W.-L., Lin, J.-F., 2012. Stress-strain analysis for evaluating the effect of the orientation of dentin tubules on their mechanical properties and deformation behavior. J. Mech. Behav. Biomed. Mater. 12, 1–8. https://doi.org/10.1016/j.jmbbm.2012.03.009.

He, L.H., Fujisawa, N., Swain, M.V., 2006. Elastic modulus and stress-strain response of human enamel by nano-indentation. Biomaterials 27 (24), 4388–4398. https://doi.org/10.1016/j.biomaterials.2006.03.045.

He, L.-H., Swain, M.V., 2009. Nanoindentation creep behavior of human enamel. J. Biomed. Mater. Res. Part A 91 (2), 352–359. https://doi.org/10.1002/jbm.a.32223.

Jakes, J.E., Frihart, C.R., Beecher, J.F., Moon, R.J., Stone, D.S., 2008. Experimental method to account for structural compliance in nanoindentation measurements. J. Mater. Res. 23 (4), 1113–1127. https://doi.org/10.1557/jmr.2008.0131.

Jameson, M.W., Hood, J.A.A., Tidmarsh, B.G., 1993. The effects of dehydration and rehydration on some mechanical properties of human dentine. J. Biomech. 26 (9), 1055–1065.

Jeng, Y.-R., Lin, T.-T., Hsu, H.-M., Chang, H.-J., Shieh, D.-B., 2011. Human enamel rod presents anisotropic nanotribological properties. J. Mech. Behav. Biomed. Mater. 4 (4), 515–522. https://doi.org/10.1016/j.jmbbm.2010.12.002.

Ji, B., Gao, H., 2004. Mechanical properties of nanostructure of biological materials. J. Mech. Phys. Solids 52 (9), 1963–1990. https://doi.org/10.1016/j.jmps.2004.03.006.

Jíra, A., Němeček, J., 2014. Nanoindentation of human tooth dentin. Key Eng. Mater. 606, 133–136. https://doi.org/10.4028/www.scientific.net/KEM.606.133.

Kahler, W., 2008. The cracked tooth conundrum: terminology, classification, diagnosis, and management. Am. J. Dent. 21 (5), 275–282.

Ketterl, W., 1961. The dentin in permanent human teeth. Stoma 14, 79–96.

Kinney, J.H., Balooch, M., Marshall, G.W., Marshall, S.J., 1999. A micromechanics model of the elastic properties of human dentine. Arch. Oral Biol. 44 (10), 813–822. https://doi.org/10.1016/s0003-9969(99)00080-1.

Koutsi, V., Noonan, R.G., Horner, J.A., Simpson, M.D., Matthews, W.G., Pashley, D.H., 1994. The effect of dentin depth on the permeability and ultrastructure of primary molars. Pediatr. Dent. 16 (1), 29–35.

Kruzic, J.J., Nalla, R.K., Kinney, J.H., Ritchie, R.O., 2003. Crack blunting, crack bridging and resistance-curve fracture mechanics in dentin: effect of hydration. Biomaterials 24 (28), 5209–5221.

Kundanati, L., D'Incau, M., Bernardi, M., Scardi, P., Pugno, N.M., 2019. A comparative study of the mechanical properties of a dinosaur and crocodile fossil teeth. J. Mech. Behav. Biomed. Mater. 97, 365–374. https://doi.org/10.1016/j.jmbbm.2019.05.025.

Lopes, M.B., Sinhoreti, M.A.C., Gonini Júnior, A., Consani, S., McCabe, J.F., 2009. Comparative study of tubular diameter and quantity for human and bovine dentin at different depths. Brazilian Dental J. 20 (4), 279–283. https://doi.org/10.1590/s0103-64402009000400003.

MacDougall, M., Slavkin, H.C., Zetchner-David, M., 1992. Characteristics of phosphorylated and non-phosphorylated dentine phosphoprotein. Biochem. J 287 (2), 651–655. https://doi.org/10.1042/bj2870651.

Mahoney, E., Holt, A., Swain, M., Kilpatrick, N., 2000. The hardness and modulus of elasticity of primary molar teeth: An ultra-micro-indentation study. J. Dent. 28 (8), 589–594.

Mahoney, E.K., Rohanizadeh, R., Ismail, F.S.M., Kilpatrick, N.M., Swain, M.V., 2004. Mechanical properties and microstructure of hypomineralised enamel of permanent teeth. Biomaterials 25 (20), 5091–5100. https://doi.org/10.1016/j.biomaterials.2004.02.044.

Marshall, G.W., Marshall, S.J., Kinney, J.H., Balooch, M., 1997. The dentin substrate: structure and properties related to bonding. J. Dent. 25 (6), 441–458.

Mencik, J. (1992). *Strength and fracture of glass and ceramics. Glass science and technology, vol. 12.* Elsevier.

Mjör, I.A., Nordahl, I., 1996. The density and branching of dentinal tubules in human teeth. Arch. Oral Biol. 41 (5), 401–412.

Mlakar, N., Pavlica, Z., Petelin, M., Štrancar, J., Zrimšek, P., Pavlič, A., 2014. Animal and human dentin microstructure and elemental composition. Central Eur. J. Med. 9 (3), 468–476. https://doi.org/10.2478/s11536-013-0295-x.

Nanci, A., 2013a. Dentin-pulp complex. In: Nanci, A. (Ed.), Ten Cate's Oral Histology, 8th ed.,. Elsevier, pp. 165–204.

Nanci, A., 2013b. Enamel: composition, formation and structure. In: Nanci, A. (Ed.), Ten Cate's Oral Histology, 8th ed.,. Elsevier, pp. 122–164.

Oliver, W.C., Pharr, G.M., 1992. An improved technique for determining hardness and elastic modulus using load and displacement sensing indentation experiments. J. Mater. Res. 7 (6), 1564–1583.

Oliver, W., Pharr, G., 2004. Measurement of hardness and elastic modulus by instrumented indentation: advances in understanding and refinements to methodology. J. Mater. Res. 19 (01), 3–20. https://doi.org/10.1557/jmr.2004.19.1.3.

Olsson, S., Öilo, G., Adamczak, E., 1993. The structure of dentin surfaces exposed for bond strength measurements. Eur. J. Oral Sci. 101 (3), 180–184.

Park, S., Wang, D.H., Zhang, D., Romberg, E., Arola, D., 2008. Mechanical properties of human enamel as a function of age and location in the tooth. J. Mater. Sci. - Mater. Med. 19 (6), 2317–2324. https://doi.org/10.1007/s10856-007-3340-y.

Pashley, D., Okabe, A., Parham, P., 1985. The relationship between dentin microhardness and tubule density. Dent. Traumatol. 1 (5), 176–179.

Qin, Q.H., Swain, M.V., 2004. A micro-mechanics model of dentin mechanical properties. Biomaterials 25 (20). https://doi.org/10.1016/j.biomaterials.2003.12.042.

Reed, R., Xu, C., Liu, Y., Gorski, J.P., Wang, Y., Walker, M.P., 2015. Radiotherapy effect on nano-mechanical properties and chemical composition of enamel and dentine. Arch. Oral Biol. 60 (5), 690–697. https://doi.org/10.1016/j.archoralbio.2015.02.020.

Reuss, A., 1929. Berechnung der Fließgrenze von Mischkristallen auf Grund der Plastizitätsbedingung für Einkristalle. ZAMM – J. Appl. Math. Mech./Zeitschrift Für Angewandte Mathematik Und Mechanik 9 (1), 49–58. https://doi.org/10.1002/zamm.19290090104.

Robb, L., Marx, J., Steenkamp, G., van Heerden, W.F.P., Pretorius, E., Boy, S.C., 2007. Scanning electron microscopic study of the dentinal tubules in dog canine teeth. J. Vet. Dent. 24 (2), 86–89.

Ryou, H., Romberg, E., Pashley, D.H., Tay, F.R., Arola, D., 2012. Nanoscopic dynamic mechanical properties of intertubular and peritubular dentin. J. Mech. Behav. Biomed. Mater. 7, 3–16.

Schilke, R., Lisson, J.A., Bauß, O., Geurtsen, W., 2000. Comparison of the number and diameter of dentinal tubules in human and bovine dentine by scanning electron microscopic investigation. Arch. Oral Biol. 45 (5), 355–361. https://doi.org/10.1016/S0003-9969(00)00006-6.

Shen, L., Barbosa de Sousa, F., Tay, N., Lang, T.S., Kaixin, V.L., Han, J., Kilpatrick-Liverman, L., Wang, W., Lavender, S., Pilch, S., Gan, H.Y., 2020. Deformation behavior of normal human enamel: A study by nanoindentation. J. Mech. Behav. Biomed. Mater. 108, 103799 https://doi.org/10.1016/j.jmbbm.2020.103799.

Tronstad, L., 1973. Ultrastructure observations on human coronal dentin. Scandanavian J. Dental Res. 81, 101–111.

Voigt, W., 1889. Ueber die Beziehung zwischen den beiden Elasticitätsconstanten isotroper Körper. Ann. Phys. 274 (12), 573–587. https://doi.org/10.1002/andp.18892741206.

Wang, R., Weiner, S., 1997. Strain-structure relations in human teeth using Moire fringes. J. Biomech. 31 (2), 135–141. https://doi.org/10.1016/S0021-9290(97)00131-0.

Wang, Y., Qin, Q.-H., 2007. A generalized self consistent model for effective elastic moduli of human dentine. Compos. Sci. Technol. 67 (7), 1553–1560. https://doi.org/10.1016/j.compscitech.2006.07.014.

Watanabe, L.G., Marshall, G.W., Marshall, S.J., 1996. Dentin shear strength: effects of tubule orientation and intratooth location. Dental Mater.: Official Publication Acad. Dental Mater. 12 (2), 109–115. https://doi.org/10.1016/S0109-5641(96)80077-7.

Whittaker, D.K., Kneale, M.J., 1979. The dentine-predentine interface in human teeth. A scanning electron microscope study. Br. Dent. J. 146 (2), 43–46. https://doi.org/10.1038/sj.bdj.4804196.

Yi, Q., Feng, X., Zhang, C., Wang, X., Wu, X., Wang, J., Cui, F., Wang, S., 2020. Comparison of dynamic mechanical properties of dentin between deciduous and permanent teeth. Connect. Tissue Res. 1–9 https://doi.org/10.1080/03008207.2020.1758684.

Zafar, M.S., Ahmed, N., 2015. The effects of acid etching time on surface mechanical properties of dental hard tissues. Dent. Mater. J. 34 (3), 315–320. https://doi.org/10.4012/dmj.2014-083.

Zhang, Y.-R.-R., Du, W., Zhou, X.-D.-D., Yu, H.-Y.-Y., 2014. Review of research on the mechanical properties of the human tooth. Int. J. Oral Sci. 6 (2), 61–69. https://doi.org/10.1038/ijos.2014.21.

Ziskind, D., Hasday, M., Cohen, S.R., Wagner, H.D., 2011. Young's modulus of peritubular and intertubular human dentin by nano-indentation tests. J. Struct. Biol. 174 (1), 23–30.